A bulk-mass-modeling-based method for retrieving Particulate Matter Pollution using CALIOP observations

Travis D. Toth[1], Jianglong Zhang[2], Jeffrey S. Reid[3], and Mark A. Vaughan[1]

[1]NASA Langley Research Center, Hampton, VA
[2]Department of Atmospheric Sciences, University of North Dakota, Grand Forks, ND
[3]Marine Meteorology Division, Naval Research Laboratory, Monterey, CA

Correspondence to: Travis D. Toth (travis.d.toth@nasa.gov); Jianglong Zhang (jianglong.zhang@und.edu)

Abstract. In this proof-of-concept paper, we apply a bulk-mass-modeling method using observations from the NASA Cloud-Aerosol Lidar with Orthogonal Polarization (CALIOP) instrument for retrieving particulate matter (PM) concentration over the contiguous United States (CONUS) over a 2-year period (2008-2009). Different from previous approaches that rely on empirical relationships between aerosol optical depth (AOD) and $PM_{2.5}$ (PM with particle diameters less than 2.5 μm), for the first time, we derive $PM_{2.5}$ concentrations, both at daytime and nighttime, from near surface CALIOP aerosol extinction retrievals using bulk mass extinction coefficients and model-based hygroscopicity. Preliminary results from this 2-year study conducted over the CONUS show a good agreement ($r^2 \sim 0.48$; mean bias of -3.3 μg m^{-3}) between the averaged nighttime CALIOP-derived $PM_{2.5}$ and ground-based $PM_{2.5}$ (with a lower r^2 of ~0.21 for daytime; mean bias of -0.4 μg m^{-3}), suggesting that PM concentrations can be obtained from active-based spaceborne observations with reasonable accuracy. Results from sensitivity studies suggest that accurate aerosol typing is needed for applying CALIOP measurements for $PM_{2.5}$ studies. Lastly, the e-folding correlation length for surface $PM_{2.5}$ is found to be around 600 km for the entire CONUS (~300 km for Western CONUS and ~700 km for Eastern CONUS), indicating

that CALIOP observations, although sparse in spatial coverage, may still be applicable for $PM_{2.5}$ studies.

1 Introduction

During the last decade, an extensive number of studies have researched the feasibility of estimating $PM_{2.5}$ (particulate matter with particle diameters smaller than 2.5 μm) pollution with the use of passive-based satellite-derived aerosol optical depth (AOD; e.g., Liu et al., 2007; Hoff and Christopher, 2009; van Donkelaar et al., 2015). Monitoring of PM concentration from space observations is needed, as $PM_{2.5}$ pollution is one of the known causes of respiratory related diseases as well as other health related issues (e.g., Liu et al., 2005; Hoff and Christopher, 2009; Silva et al., 2013). Yet, ground-based $PM_{2.5}$ measurements are often inconsistent or have limited availability over much of the globe.

In some earlier studies, empirical relationships of $PM_{2.5}$ concentrations and AODs were developed and used for estimating $PM_{2.5}$ concentrations from passive sensor retrieved AODs (e.g., Wang and Christopher, 2003; Engel-Cox et al., 2004; Liu et al., 2005; Kumar et al., 2007; Hoff and Christopher, 2009). One of the limitations of this approach is that vertical distributions and thermodynamic state of aerosol particles vary with space and time. Especially for regions with elevated aerosol plumes, deep boundary layer entrainment zones, or strong nighttime inversions, column-integrated AODs are not a good approximation of surface $PM_{2.5}$ concentrations at specific points and times (e.g., Liu et al., 2004; Toth et al., 2014; Reid et al., 2017). Indeed, Kaku et al. (2018) recently showed that surface $PM_{2.5}$ had longer spatial correlation lengths than AOD, even in the "well behaved" southeastern United States where previous studies showed good correlation between $PM_{2.5}$ and AOD (e.g., Wang and Christopher, 2003). To account for variability in aerosol

55 vertical distribution, several studies have attempted the use of chemical transport models, or CTMs
56 (e.g., van Donkelaar et al., 2015). Satellite data assimilation of AOD has become commonplace,
57 vastly improving AOD analyses and short-term prediction (e.g., Zhang et al., 2014; Sessions et al.,
58 2015). Yet, $PM_{2.5}$ simulations remain poor (e.g., Reid et al., 2016). Uncertainties in such studies
59 are unavoidable due to uncertainties in CTM-based aerosol vertical distributions, and no nighttime
60 AODs are currently available from passive-based satellite retrievals.

61 It is arguable that from a climatological/long-term average perspective, the use of AOD as
62 a proxy for $PM_{2.5}$ concentrations nevertheless has certain qualitative skill (e.g., Toth et al., 2014;
63 Reid et al., 2017) due to the averaging process that suppresses sporadic aerosol events with highly
64 variable vertical distributions. Still, as illustrated in Fig. 1, where 2-year (2008-2009) means of
65 Moderate Resolution Imaging Spectroradiometer (MODIS) AOD are plotted against $PM_{2.5}$
66 concentrations throughout the contiguous United States (CONUS), although a linear relationship
67 is plausibly shown, a low r^2 value of 0.08 is found. To construct Fig. 1, Aqua MODIS Collection
68 6 (C6) Optical_Depth_Land_And_Ocean data (0.55 μm), restricted to "Very Good" retrievals as
69 reported by the Land_Ocean_Quality_Flag, are first collocated with daily surface $PM_{2.5}$
70 measurements in both space and time (i.e., within 40 km in distance and the same day), and then
71 collocated daily pairs are averaged into 2-year means (for each $PM_{2.5}$ site). Figure 1 may be
72 indicating that even from a long-term mean perspective, aerosol vertical distributions are not
73 uniform across the CONUS, which is also confirmed by other studies (e.g., Toth et al., 2014).
74 AOD retrievals themselves, with known uncertainties due to cloud contamination and assumptions
75 in the retrieval process (e.g., Levy et al., 2013), may also introduce uncertainties to that task.

76 On board the Cloud-Aerosol Lidar and Infrared Pathfinder Satellite Observations
77 (CALIPSO) satellite, the Cloud-Aerosol Lidar with Orthogonal Polarization (CALIOP) instrument

provides observations of aerosol and cloud vertical distributions at both day and night (Hunt et al., 2009; Winker et al., 2010). Given that CALIOP provides aerosol extinction retrievals near the ground, it is interesting and reasonable to raise the question: can near surface CALIPSO extinction be used as a better physical quantity than AOD for estimating surface $PM_{2.5}$ concentrations? This is because unlike AOD, which is a column-integrated value, near surface CALIPSO extinction is, in theory, a more realistic representation of near surface aerosol properties. Yet, in comparing with passive sensors such as MODIS, which has a swath width on the order of ~2000 km, CALIOP is a nadir pointing instrument with a narrow swath of ~70 m and a repeat cycle of 16 days (Winker et al., 2009). Thus, the spatial sampling of CALIOP is sparse on a daily basis and temporal sampling or other conditional or contextual biases are unavoidable if CALIOP observations are used to estimate daily $PM_{2.5}$ concentrations (Zhang and Reid, 2009; Colarco et al., 2014). Also, there are known uncertainties in CALIPSO retrieved extinction values due to uncertainties in the retrieval process, such as the lidar ratio (extinction-to-backscatter ratio), calibration, and the "retrieval fill value" (RFV) issue (Young et al., 2013; Toth et al., 2018).

Even with these known issues, especially the sampling bias, it is still compelling to investigate if near surface CALIOP extinction can be utilized to retrieve surface $PM_{2.5}$ concentrations with reasonable accuracy from a long-term (i.e., two-year) mean perspective. CALIOP data have been successfully used in $PM_{2.5}$ studies in the past, but primarily for assisting passive-based AOD/$PM_{2.5}$ analyses using aerosol vertical distribution as a constraint (e.g., Glantz et al., 2009; van Donkelaar et al., 2010; Val Martin et al., 2013; Toth et al., 2014; Li et al., 2015; Gong et al., 2017). However, the question remained as to the efficacy of the direct use of CALIOP retrievals. To demonstrate a concept, we developed a bulk mass scattering scheme for inferring PM concentrations from near surface aerosol extinction retrievals derived from CALIOP

observations. The bulk method used here is based upon the well-established relationship between particle light scattering and $PM_{2.5}$ aerosol mass concentration (e.g., Charlson et al., 1968; Waggoner and Weiss, 1980; Liou, 2002; Chow et al., 2006), discussed further, with the relevant equations, in Sect. 2.

In this study, using two years (2008-2009) of CALIOP and United States (U.S.) Environmental Protection Agency (EPA) data over the CONUS, the following questions are addressed:

1. Can CALIOP extinction be used effectively for estimating $PM_{2.5}$ concentrations through a bulk mass scattering scheme from a 2-year mean perspective for both daytime and nighttime?
2. Can CALIOP extinction be used as a better parameter than AOD for estimating $PM_{2.5}$ concentrations from a 2-year mean perspective?
3. What are the sampling biases we can expect in CALIOP estimates of $PM_{2.5}$?
4. How do uncertainties in bulk properties compare to overall CALIOP-retrieved $PM_{2.5}$ uncertainty?

Details of the methods and datasets used are described in Sect. 2. Section 3 shows the preliminary results using two years of EPA $PM_{2.5}$ and CALIOP data, including an uncertainty analysis. The conclusions of this paper are provided in Sect. 4.

2 Data and Methods

123 Since 1970, the U.S. EPA has monitored surface PM using a number of Federal
124 Reference/Equivalent Methods (FRMs/FEMs), which employ gravimetric, tapered element
125 oscillating microbalance (TEOM), and beta gauge instruments (Federal Register, 1997;
126 Greenstone, 2002). Two years (2008-2009) of daily $PM_{2.5}$ Local Conditions (EPA code = 88101)
127 data were acquired from the EPA Air Quality System for use in this investigation, consistent with
128 our previous $PM_{2.5}$ study (Toth et al., 2014). These data represent $PM_{2.5}$ concentrations over a 24-
129 hour period and include two scenarios: one sample is taken during the 24-hour duration (i.e., filter-
130 based measurement), or an average is computed from hourly samples within this time period (every
131 hour may not have an available measurement, however).
132 Note that uncertainties have been reported for hourly PM measurements (Kiss et al., 2017).
133 Examples of some uncertainties in these $PM_{2.5}$ measurements depend upon the instrument/method
134 used: gravimetric (e.g., transport to the lab/human error and volatization of PM during the drying
135 process; Patashnick et al., 2001), TEOM (e.g., errors due to improper inlet tube temperature;
136 Eatough et al., 2003), and beta attenuation monitors (e.g., changes in the sample flow rate due to
137 variations in temperature and moisture; Spagnolo, 1989). Also, it has been found that beta
138 attenuation monitors may be more accurate than TEOM, as TEOM can underestimate $PM_{2.5}$ at low
139 temperatures (e.g., Chung et al., 2001). Still, as suggested by Kiss et al. (2017), PM data collected
140 over a longer period of time are much less likely to be biased. Thus, we expect lower uncertainties
141 from data collected over 24-hours, then daily data generated by averaging hourly observations.
142 Fully quantifying the differences from the two different PM observing methods, however, is the
143 subject for a future study.
144 CALIOP, flying aboard the CALIPSO platform within the A-Train satellite constellation,
145 is a dual wavelength (0.532 and 1.064 μm) lidar that has collected profiles of atmospheric aerosol

146 particles and clouds since summer 2006 (Winker et al., 2007). In this study, daytime and nighttime
147 extinction coefficients retrieved at 0.532 μm from the Version 4.10 CALIOP Level 2 5 km aerosol
148 profile (L2_05kmAPro) product were used. Using parameters provided in the L2_05kmAPro
149 product, as well as the corresponding Level 2 5 km aerosol layer (L2_05kmALay) product, a robust
150 quality-assurance (QA) procedure for the aerosol observations was implemented (Table 1).
151 Further information on the QA metrics and screening protocol are discussed in detail in previous
152 studies (Kittaka et al. 2011; Campbell et al. 2012; Toth et al. 2013; 2016). Once the QA procedure
153 was applied, the aerosol profiles were linearly re-gridded from 60 m vertical resolution (above
154 mean sea level [AMSL]) to 100 m segments (i.e., resampled to 100 m resolution) referenced to the
155 local surface (above ground level [AGL]; Toth et al., 2014; 2016). The choice of 100 m was
156 arbitrary, and the profiles were re-gridded in order to obtain an AGL-corrected dataset, as opposed
157 to the AMSL-referenced profiles provided by the L2_05kmAPro product. Surface elevation and
158 relative humidity (RH) were taken from collocated model data included in the CALIPSO
159 L2_05kmAPro product (CALIPSO Data Products Catalog (Release 4.20); RH taken from the
160 Modern Era Retrospective-Analysis for Research, or MERRA-2 reanalysis product). To limit the
161 effects of signal attenuation and increase the chances of measuring aerosol presence near the
162 surface, the Atmospheric Volume Description parameter within the L2_05kmAPro dataset is used
163 to cloud-screen each aerosol profile as in Toth et al. (2018).

164 In this study, near surface PM mass concentration (C_m) is derived from near surface
165 CALIOP extinction based on a bulk formulation as in Equation 1 (e.g., Liou, 2002; Chow et al.,
166 2006):

167 $$\beta = C_m(a_{scat}f_{rh} + a_{abs}) \times 1000 \quad (1)$$

where β is CALIOP-derived near surface extinction in km^{-1}, C_m is the PM mass concentration in $\mu g\ m^{-3}$, a_{scat} and a_{abs} are dry mass scattering and absorption efficiencies in $m^2\ g^{-1}$, and f_{rh} represents the light scattering hygroscopicity, respectively. As a preliminary study, for the purpose of demonstrating this concept, we assume the dominant aerosol type over the contiguous U.S. (CONUS) is pollution aerosol (i.e., the most prevalent near-surface aerosol type reported in the CALIOP products for the CONUS during 2008-2009 is polluted continental) with a_{scat} and a_{abs} values of 3.40 and 0.37 $m^2\ g^{-1}$ (Hess et al., 1998; Lynch et al., 2016), respectively. These values are similar to those reported in Malm and Hand (2007) and Kaku et al. (2018) but are interpolated to 0.532 μm from values at 0.450 μm and 0.550 μm obtained from the Optical Properties of Aerosols and Clouds (OPAC) model (Hess et al., 1998). Still, both a_{scat} and a_{abs} have regional and species related dependencies. Also, only 2-year averages are used in this study, and we assume that sporadic aerosol plumes are smoothed out in the averaging process, and that bulk aerosol properties are similar throughout the study region. We have further explored the impact of aerosol types to $PM_{2.5}$ retrievals in a later section. Furthermore, to aid in focusing this study on fine mode/anthropogenic aerosols, those aerosol extinction range bins classified as dust by the CALIOP typing algorithm were excluded from the analysis.

Also, surface PM concentrations are dry mass measurements. To account for the impact of humidity on a_{scat} (it is assumed that a_{abs} is not affected by moisture; Nessler et al., 2005; Lynch et al., 2016), we estimated the hygroscopic growth factor for pollution aerosol based on Hanel (1976), as shown in Equation 2:

$$f_{rh} = \left(\frac{1 - RH}{1 - RH_{ref}}\right)^{-\Gamma} \quad (2)$$

where f_{rh} is the hygroscopic growth factor, RH is the relative humidity, and RH_{ref} is the reference RH and is set to 30% in this study (Lynch et al., 2016). Γ is a unitless value (a fit parameter describing the amount of hygroscopic increase in scattering) and is assumed to be 0.63 (i.e., sulfate aerosol) in this study (Hanel, 1976; Chew et al., 2016; Lynch et al., 2016).

Additionally, the CALIOP-derived PM density is for all particle sizes. To convert from mass concentration of PM (C_m) to mass concentration of $PM_{2.5}$ ($C_{m2.5}$), which represents mass concentration for particle diameters smaller than 2.5 μm, we adopted the $PM_{2.5}$ to PM_{10} (PM with diameters less than 10 μm) ratio (ϕ) of 0.6 as measured during the Studies of Emissions and Atmospheric Composition, Clouds and Climate Coupling by Regional Surveys ($SEAC^4RS$) campaign over the US (Kaku et al., 2018). Again, the ratio of $PM_{2.5}$ to PM_{10} can also vary spatially, however we used a regional mean to demonstrate the concept. Analyses in a later section using two-years (2008-2009) of surface $PM_{2.5}$ to PM_{10} data suggest that 0.6 is a rather reasonable number to use for the CONUS for the study period. Here we assume that mass concentrations for particle diameters larger than 10 μm are negligible over the CONUS. Thus, we can rewrite Equation 1 as:

$$C_{m2.5} = \frac{\beta \times \phi}{(a_{scat} \times f_{rh} + a_{abs}) \times 1000} \qquad (3)$$

where $C_{m2.5}$ is the CALIOP-derived $PM_{2.5}$ concentration in units of $\mu g\ m^{-3}$.

Lastly, we note that most of the results are shown in the form of scatter plots with fits from Deming regression (Deming, 1943). Due to uncertainties in $PM_{2.5}$ data, we show slopes computed from Deming regression analyses instead of those from simple linear regression. Deming regression in particular is appropriate here, as it accounts for errors in both the independent and dependent variables (Deming, 1943), and has been used in past $PM_{2.5}$ related studies (e.g., Huang et al., 2014).

3 Results and Discussion

3.1 Regional analysis

Figure 2a shows the mean $PM_{2.5}$ concentration using two years (2008-2009) of daily surface $PM_{2.5}$ data from the U.S. EPA ($PM_{2.5\_EPA}$), not collocated with CALIOP observations. A total of 1,091 stations (some operational throughout the entire period; others only partially) are included in the analysis and observations from those stations are further used in evaluating CALOP-derived $PM_{2.5}$ concentrations ($C_{m2.5}$), as later shown in Fig. 3. $PM_{2.5}$ concentrations of ~10 μg m^{-3} are found over the eastern CONUS. In comparison, much lower $PM_{2.5}$ concentrations of ~5 μg m^{-3} are exhibited for the interior CONUS, over states including Montana, Wyoming, North Dakota, South Dakota, Utah, Colorado, and Arizona. For the west coast of the CONUS, and especially over California, higher $PM_{2.5}$ concentrations are observed, with the maximum two-year mean near 20 μg m^{-3}. Note that the spatial distribution of surface $PM_{2.5}$ concentrations over the CONUS as shown in Fig. 2a is consistent with reported values from several studies (e.g., Hand et al., 2013; Van Donkelaar et al., 2015; Di et al., 2017).

Figure 3a shows the two-year averaged 1° x 1° (latitude/longitude) gridded daytime CALIOP aerosol extinction over the CONUS using CALIOP observations from 100-1000 m, referenced to the number of cloud-free L2_05kmAPro profiles in each 1 x 1° bin. The lowest 100 m of CALIOP extinction data are not used in the analysis due to the potential of surface return contamination (e.g., Toth et al., 2014), although this has been improved for the Version 4 CALIOP products but may still be present in some cases. Here the averaged extinction from 100-1000 m is used to represent near surface aerosol extinction. This selection of the 100-1000 m layer is somewhat arbitrary, even though it is estimated from the mean CALIOP-based aerosol vertical distribution over the CONUS (Toth et al., 2014). Thus, a sensitivity study is provided in a later

section to understand the impact of this aerosol layer selection to CALIOP-based $PM_{2.5}$ retrievals. As shown in Fig. 3a, higher mean near surface CALIOP extinction of 0.1 km^{-1} are found for the eastern CONUS and over California, while lower values of 0.025-0.05 km^{-1} found for the interior CONUS. Figure 3b shows a plot similar to Fig. 3a but using nighttime CALIOP observations only. Although similar spatial patterns are found during both day and night, the near surface extinction values are overall lower for nighttime than daytime, and nighttime data are less noisy than daytime. These findings are not surprising, as daytime CALIOP measurements are subject to contamination from background solar radiation (e.g., Omar et al., 2013).

To investigate any diurnal biases in the data, Figs. 3c and 3d show the derived $PM_{2.5}$ concentration using daytime and nighttime CALIOP data respectively, based on the method described in Section 2. Both Figures 3c and 3d suggest a higher $PM_{2.5}$ concentration of ~10-12.5 $\mu g\ m^{-3}$ over the eastern CONUS, and a much lower $PM_{2.5}$ concentration of ~2.5-5 $\mu g\ m^{-3}$ over the interior CONUS. High $PM_{2.5}$ values of 10-20 $\mu g\ m^{-3}$ are also found over the west coast of the CONUS, particularly over California. The spatial distribution of $PM_{2.5}$ concentrations, as derived using near surface CALIOP data (Figs. 3c and 3d, as well as the combined daytime and nighttime perspective shown in Fig. 2c), is remarkably similar to the spatial distribution of $PM_{2.5}$ values as estimated based on ground-based observations (Fig. 2a). Still, day and night differences in $PM_{2.5}$ concentrations are also clearly visible, as higher $PM_{2.5}$ values are found, in general, during daytime, based on CALIOP observations. The high daytime $PM_{2.5}$ values, as shown in Fig. 3c, may represent stronger near surface convection and more frequent anthropogenic activities during daytime. However, they may also be partially contributed from solar radiation contamination. Another possibility is that the daytime mean extinction coefficients (from which the mean $PM_{2.5}$ estimates are derived) appear artifically larger than at night due to high daytime noise limiting the

ability of CALIOP to detect fainter aerosol layers during daylight operations. Note that, for context, maps of the number of days and CALIOP Level 2 5 km aerosol profiles used in the creation of Fig. 3a-d are shown in Appendix Fig. 1.

Figure 3e shows the inter-comparison between $PM_{2.5\_EPA}$ and $PM_{2.5\_CALIOP}$ concentrations. Note that only CALIOP and ground-based $PM_{2.5}$ data pairs, which are within 100 km of each other and have reported values for the same day (i.e., year, month, and day), are used to generate Fig. 3e. Still, although only spatially and temporally collocated data pairs are used, ground-based $PM_{2.5}$ data represent 24-hour averages, while CALIOP-derived $PM_{2.5}$ concentrations are instantaneous values over the daytime CALIOP overpass. To reduce this temporal bias, two years (2008-2009) of collocated CALIOP-derived and measured $PM_{2.5}$ concentrations are averaged and only the two-year averages are used in constructing Fig 3e. Also, to minimize the above-mentioned temporal sampling bias, ground stations with fewer than 100 collocated pairs are discarded. This leaves a total of 276 stations for constructing Fig. 3e.

As shown in Fig. 3e, an r^2 value of 0.21 (with slope of 1.07) is found between CALIOP-derived and measured surface $PM_{2.5}$ concentrations, with a corresponding mean bias of -0.40 $\mu g\ m^{-3}$ ($PM_{2.5\_CALIOP}$ - $PM_{2.5\_EPA}$). In comparison, Fig. 3f shows results similar to Fig. 3e, but for nighttime CALIOP data. A much higher r^2 value of 0.48 (with slope of 0.96) is found between CALIOP-derived and measurement $PM_{2.5}$ values from 528 EPA stations, with a corresponding mean bias of -3.3 μgm^{-3} ($PM_{2.5\_CALIOP}$ - $PM_{2.5\_EPA}$). This may be related to the diurnal variability of $PM_{2.5}$ concentrations, as the daily mean EPA measurement might be closer to the CALIOP A.M. retrieval than to its P.M. counterpart. Still, data points are more scattered in Fig. 3e in comparison with Fig. 3f, which again indicates that daytime CALIOP data are noisier, possibly due to daytime

280 solar contamination as well as other factors such as biases in relative humidity. Details of these
281 biases are further explored in Section 3.2.

282 To supplement this analysis, a pairwise $PM_{2.5\_EPA}$ and $PM_{2.5\_CALIOP}$ (day and night CALIOP
283 combined) analysis is presented in the spatial plots of Figs. 2b and 2d. Here, however, we lift the
284 100 collocated pairs requirement to increase data samples for better spatial representativeness. The
285 spatial variability of $PM_{2.5}$ over the CONUS is consistent with the observed patterns of non-
286 collocated data (i.e., Figs. 2a and 2c), but with generally higher values due to differences in
287 sampling. Also, comparing Figs. 2b and 2d, $PM_{2.5\_EPA}$ spatial patterns match well with those of
288 $PM_{2.5\_CALIOP}$, yet with larger values for $PM_{2.5\_EPA}$ (consistent with the biases discussed above).
289 Lastly, a scatterplot of the pairwise analysis shown in Figs. 2b and 2d is provided in Fig. 4. An r^2
290 value of 0.40 is found between EPA and CALIOP-derived $PM_{2.5}$ concentrations from a combined
291 daytime and nighttime CALIOP perspective. Overall, Figs. 2, 3, and 4 indicate that near surface
292 CALIOP extinction data can be used to estimate surface $PM_{2.5}$ concentrations with reasonable
293 accuracy.

294

295 **3.2 Uncertainty analysis**

296 In this section, uncertainties in the CALIOP derived, 2-year averaged $PM_{2.5}$ concentrations
297 are explored as functions of aerosol vertical distribution, $PM_{2.5}$ to PM_{10} ratio, RH, aerosol type,
298 and cloud presence above. Spatial sampling related biases as well as prognostic errors are also
299 studied.

300

301 **3.2.1 Prognostic errors in $C_{m2.5}$**

As a first step for the uncertainty analysis, we estimated the prognostic error of 2-year averaged $PM_{2.5\_CALIOP}$. Figure 5 shows the root-mean-square error (RMSE) of CALIOP-based $PM_{2.5}$ concentrations against those from EPA stations as a function of CALIOP-based $PM_{2.5}$ for the 2008-2009 period over the CONUS. RMSEs were computed for five equally sampled bins, determined from a cumulative histogram analysis. Each point in Fig. 5, from left to right, represents the RMSE and mean $PM_{2.5}$ concentration derived from CALIOP for 0-20%, 20-40%, 40-60%, 60-80%, and 80-100% cumulative frequencies. A mean combined daytime and nighttime RMSE of ~4 μg m^{-3} is found, with a mean value slightly greater for nighttime (~4.3 μg m^{-3}) than daytime (~3.7 μg m^{-3}). While most bins exhibit larger nighttime RMSEs, daytime RMSEs are larger for the greatest mean CALIOP-derived $PM_{2.5}$ concentrations.

3.2.2 Surface layer height sensitivity study

A sensitivity study was conducted for which $PM_{2.5}$ was derived from near-surface CALIOP aerosol extinction by varying the height of the surface layer in increments of 100 m from the ground to 1000 m. Note that the surface layer (0-100 m) is included for this sensitivity study only. The statistical results of this analysis, for both daytime and nighttime conditions, are shown in Table 2. Four statistical parameters were computed, consisting of r^2, slope from Deming regression, mean bias (CALIOP – EPA) of $PM_{2.5}$, and percent error change in derived $PM_{2.5}$, defined as: ((mean_new_$PM_{2.5}$ – mean_original_$PM_{2.5}$)/mean_original_$PM_{2.5}$)*100. For context, the bottom row of Table 2 shows the results from the original analysis. In terms of r^2 and slope, optimal values peak at different surface layer heights between daytime and nighttime. For example, for daytime, the largest correlations are found for the 0-600 m and 0-700 m layers, while

for nighttime these are found for the 0-300 m and 0-400 m layers. However, the 0-300 m layer exhibits the lowest mean bias for the daytime analysis, and the 100-1000 m layer exhibits the lowest mean bias for the nighttime analysis. Overall, marginal changes are found for varying the height of the surface layer. Yet the largest mean bias is found for the 0-100 m layer, indicating the need for excluding the 0-100 m layer in the analysis.

3.2.3 RH sensitivity study

Profiles of RH were taken from the MERRA-2 reanalysis product, as these collocated data are provided in the CALIPSO L2_05kmAPro product. However, biases may exist in this RH dataset. Thus, we examined the impact of varying the RH values by +/- 10% on the CALIOP-derived $PM_{2.5}$ concentrations. For both daytime and nighttime analyses, no significant differences in the r^2 and slope values were found. However, a +15% change in the mean derived $PM_{2.5}$ values was found by decreasing the RH values by 10%, while a -15% change in the mean derived $PM_{2.5}$ values was found by increasing the RH values by 10%.

3.2.4 $PM_{2.5}$ to PM_{10} ratio sensitivity study

Another source of uncertainty in this study is the $PM_{2.5}/PM_{10}$ ratio. Using surface-based $PM_{2.5}$ and PM_{10} data from those EPA stations over the CONUS for 2008-2009 with concurrent $PM_{2.5}$ and PM_{10} daily data available (i.e., 409 stations), we computed the mean $PM_{2.5}/PM_{10}$ ratio, and its corresponding standard deviation. The mean ratio was 0.56 with a standard deviation of 0.32. It is interesting to note that the mean $PM_{2.5}/PM_{10}$ ratio estimated from two years of surface observations over the CONUS is close to 0.6 (the number used in this study), as reported by Kaku et al. (2018). We also tested the sensitivity of the derived $PM_{2.5}$ concentrations as a function of $PM_{2.5}/PM_{10}$ ratio for two scenarios: ±1 standard deviation of the mean (Table 3). In general, a ±50

348 % to 60 % change is found with the variation of the $PM_{2.5}/PM_{10}$ ratio at the range of ±1 standard
349 deviation of the mean. As suggested from Table 3, the lowest mean daytime bias is found for a
350 ratio of 0.6, and for nighttime the lowest mean bias occurs using a ratio of 0.88.
351
352 **3.2.5 Sampling-related biases**
353 As mentioned in the introduction section, a sampling bias, due to the very small footprint
354 size and ~16 day repeat cycle of CALIOP, can exist when using CALIOP observations for $PM_{2.5}$
355 estimates (Zhang and Reid, 2009). This sampling-induced bias is investigated from a 2-year mean
356 perspective by comparing histograms of $PM_{2.5\_EPA}$ and $C_{m2.5}$ concentrations as shown in Fig. 6. To
357 generate Fig. 6, all available daily EPA $PM_{2.5}$ are used to represent the "true" 2-year mean spectrum
358 of $PM_{2.5}$ concentrations over the EPA sites. The aerosol extinction data spatially collocated to the
359 EPA sites (Sect. 3.1), but not temporally collocated, are used for estimating the 2-year mean
360 spectrum of $PM_{2.5}$ concentrations as derived from CALIOP observations. To be consistent with
361 the previous analysis, only cloud-free CALIOP profiles are considered. The $PM_{2.5\_EPA}$
362 concentrations peak at ~10 μg m^{-3} (standard deviation of ~3 μg m^{-3}), and CALIOP-derived $PM_{2.5}$
363 peaks at ~9 μg m^{-3} (daytime; standard deviation of ~4 μg m^{-3}) and ~7 μg m^{-3} (nighttime; standard
364 deviation of ~2 μg m^{-3}). The distribution shifts towards smaller concentrations for CALIOP, more
365 so for nighttime than daytime (possibly due to CALIOP daytime versus nighttime detection
366 differences).
367 Still, Fig. 6 may reflect the diurnal difference in $PM_{2.5}$ concentrations as well as the
368 retrieval bias in $C_{m2.5}$ values. Thus, we have re-performed the exercise shown in Fig. 6 using
369 spatially and temporally collocated $PM_{2.5\_EPA}$ and $C_{m2.5}$ data as shown in Fig. 7. To construct Fig.
370 7, $PM_{2.5\_EPA}$ and $C_{m2.5}$ data are collocated following the steps mentioned in Sect. 3.1, with CALIOP

and EPA $PM_{2.5}$ representing 2-year mean values for each EPA station. Again, only cloud-free CALIOP profiles are considered for this analysis. As shown in Fig. 7a, the $PM_{2.5\_EPA}$ concentrations peak at ~12 μg m^{-3} (standard deviation of ~4 μg m^{-3}), and daytime $C_{m2.5}$ peaks at ~10 μg m^{-3} (standard deviation of ~4 μg m^{-3}). In comparison, with the use of collocated nighttime $C_{m2.5}$ and $PM_{2.5\_EPA}$ data as shown in Fig. 7b, the peak $PM_{2.5\_EPA}$ value is about 5 μg m^{-3} higher than the peak $C_{m2.5}$ value (with similar standard deviations as found in the analyses of Fig. 7a). Considering both Figs. 6 and 7, it is likely that the temporal sampling bias seen in Fig. 6 is at least in part due to retrieval bias as well as the difference in $PM_{2.5}$ concentrations during daytime and nighttime.

3.2.6 CALIOP AOD analysis

Most past studies focused on the use of column AODs as proxies for surface $PM_{2.5}$ (e.g., Liu et al., 2005; Hoff and Christopher, 2009; van Donkelaar et al., 2015). Therefore, it is interesting to investigate whether near surface CALIOP extinction values can be used as a better physical quantity to estimate surface $PM_{2.5}$ in comparing with column-integrated CALIOP AOD. To achieve this goal, we have compared CALIOP column AOD and $PM_{2.5}$ from EPA stations, as shown in Fig. 8. Similar to the scatterplots of Fig. 4, each point represents a two-year mean for each EPA site, and was created from a dataset following the same spatial/temporal collocation as described above. As shown in Fig. 9, r^2 values of 0.04 and 0.13 are found using CALIOP daytime and nighttime AOD data, respectively, similar to the MODIS-based analysis shown in Fig. 1. This is expected, as elevated aerosol layers will negatively impact the relationship between surface $PM_{2.5}$ and column AOD. The derivation of surface $PM_{2.5}$ from near surface CALIOP extinction, as demonstrated from this study however, provides a much better spatial matching between the

quantities being compared, with potential error terms that can be well quantified and minimized in later studies.

3.2.7 Cloud flag sensitivity study

For most of this paper, a strict cloud screening process is implemented, during which no clouds are allowed in the entire CALIOP profile. However, in contrast to passive sensor capabilities (e.g., MODIS), near-surface aerosol extinction coefficients can be readily retrieved from CALIOP profiles even when there are transparent cloud layers above. Therefore, we conducted an additional analysis for which no cloud flag was set (i.e., all-sky conditions). Results are shown in scatterplot form in Fig. 9, in a similar manner as Figs. 3e and f, with an additional 97 points for the daytime analysis and 156 points for the nighttime analysis. Comparing the all-sky results with those of Figs. 3e, and f (cloud-free conditions), the r^2 values are similar. This is also true in terms of mean bias, with similar values of 0.70 $\mu g\ m^{-3}$ found for daytime, and -2.68 $\mu g\ m^{-3}$ for nighttime, all-sky scenarios. This indicates that our method performs reasonably well from an all-sky perspective. However, we note that restricting the analysis to solely those cases that are cloudy (not shown), the method does not perform as well. For example, the r^2 value decreases by 71% for the daytime analysis compared to the cloud-free results (Fig. 3e). The corresponding nighttime r^2 value decreases by 90%. This is expected, as any errors made in estimating the optical depths of the overlying clouds will propagate (as biases) into the extinction retrievals for the underlying aerosols.

3.2.8 Aerosol type analysis

Also, for this study, we assume that the primary aerosol type over the CONUS is pollution (i.e., sulfate) aerosol, which is generally composed of smaller (fine mode) particles that tend to exhibit mass extinction efficiencies ~4 $m^2 g^{-1}$. However, even after implementing our dust-free restriction, the study region can also be contaminated with non-pollution aerosols, which can have a larger particle size and exhibit lower mass extinction efficiencies (e.g., Hess et al., 1998; Malm and Hand, 2007; Lynch et al., 2016). The use of $PM_{2.5}$ versus PM_{10} somewhat mitigates this size dependency, but nevertheless coarse mode dust or sea salt can dominate $PM_{2.5}$ mass values (e.g., Atwood et al., 2013).

Thus, in this section, the impact of aerosol types to the derived $PM_{2.5}$ concentrations was explored by varying the mass scattering and absorption efficiencies and gamma values associated with each aerosol type. The three aerosol types chosen for this sensitivity study were dust, sea salt, and smoke, based upon Lynch et al. (2016). The mass scattering and absorption values for dust and sea salt were interpolated to 0.532 μm from values at 0.450 μm and 0.550 μm from OPAC (as was done for the sulfate case; Hess et al., 1998). For smoke, these values were interpolated to 0.532 μm from values at 0.440 μm and 0.670 μm as provided by Reid et al. (2005) for smoke cases over the US and Canada. The gamma values were taken from Lynch et al. (2016) and the references within. These values, as well as the results from this sensitivity study, are shown in Table 4. If we assume all aerosols within the study region are smoke aerosols, no major changes in the retrieved CALIOP $PM_{2.5}$ values are found. However, significant uncertainties on the order of ~200% are found if sea salt, or ~800% if dust, aerosol mass scattering/absorption efficiencies and gamma values are used instead. Clearly, this study suggests that accurate aerosol typing is necessary for future applications of CALIOP observations for surface $PM_{2.5}$ estimations.

3.3 E-folding correlation length for $PM_{2.5}$ concentrations over the CONUS

As a last study, we also estimated the spatial e-folding correlation length for $PM_{2.5}$ concentrations over the CONUS. This provides us an estimation of the correlation between a CALIOP-derived and actual $PM_{2.5}$ concentration for a given location as a function of distance between the CALIOP observation and the given location. To accomplish this, all EPA stations over the CONUS with at least 50 days of daily data available for the 2008-2009 period were first determined. Next, the distances between each pair of these EPA stations, and their corresponding correlation of daily $PM_{2.5}$ concentrations, were computed. Results are shown in Fig. 10 as a scatterplot, with individual points in gray and the black curve representing the exponential fit to the data. A decrease in $PM_{2.5}$ correlation with distance between EPA stations is found, and the e-folding length in correlation (e.g., correlation reduced to 1/e, or 0.37) is ~600 km (from an AOD standpoint, this value is 40-400 km, as suggested by Anderson et al., 2003).

Also included in Fig. 10 are results from a corresponding regional analysis, with the red and blue lines showing bin averages (10 km) for the Western and Eastern CONUS, respectively (regions partitioned by the -97° longitude line). The e-folding length is ~300 km for the Western CONUS, and ~700 km for the Eastern CONUS, indicating a much shorter correlation length for pollution over the Western CONUS, possibly due to a more complex terrain such as mountains. Overall, these $PM_{2.5}$ e-folding lengths suggest that CALIOP-derived $PM_{2.5}$ concentrations could still have some representative skill within a few hundred kilometers of a given location.

4 Conclusions

In this paper, we have demonstrated a new bulk-mass-modeling method for retrieving surface particulate matter (PM) with particle diameters smaller than 2.5 μm ($PM_{2.5}$) using

462 observations acquired by the NASA Cloud-Aerosol Lidar with Orthogonal Polarization (CALIOP)
463 instrument from 2008-2009. For the purposes of demonstrating this concept, only regionally-
464 averaged parameters, such as mass scattering and absorption coefficients, and $PM_{2.5}$ to PM_{10} (PM
465 with particle diameters smaller than 10 μm) conversion ratio, are used. Also, we assume the
466 dominant type of aerosols over the study region is pollution aerosols (supported by the occurrence
467 frequencies of aerosol types determined by the CALIOP algorithms), and exclude aerosol
468 extinction range bins classified as dust from the analysis. Even with the highly-averaged
469 parameters, the results from this paper are rather promising and demonstrate a potential for
470 monitoring PM pollution using active-based lidar observations. Specifically, the primary results
471 of this study are as follows:

472 1. CALIOP-derived $PM_{2.5}$ concentrations of ~10-12.5 μg m^{-3} are found over the eastern
473 contiguous United States (CONUS), with lower values of ~2.5-5 μg m^{-3} over the central
474 CONUS. $PM_{2.5}$ values of ~10-20 μg m^{-3} are found over the west coast of the CONUS,
475 primarily California. The spatial distribution of 2-year mean $PM_{2.5}$ concentrations derived
476 from near surface CALIOP aerosol data compares well to the spatial distribution of *in situ*
477 $PM_{2.5}$ measurements collected at the ground-based stations of the U.S. Environmental
478 Protection Agency (EPA). The use of nighttime CALIOP extinction to derive $PM_{2.5}$ results
479 in a higher correlation (r^2 = 0.48; mean bias = -3.3 μgm^{-3}) with EPA $PM_{2.5}$ than daytime
480 CALIOP extinction data (r^2 = 0.21; mean bias = -0.40 μgm^{-3}).
481 2. Correlations between CALIOP aerosol optical depth (AOD) and EPA $PM_{2.5}$ are much
482 lower (r^2 values of 0.04 and 0.13, for daytime and nighttime CALIOP AOD data,
483 respectively) than those obtained from derived $PM_{2.5}$ using near-surface CALIOP aerosol
484 extinction. A similar correlation is also found between Moderate Resolution Imaging

Spectroradiometer (MODIS) AOD and EPA $PM_{2.5}$ from two-year (2008-2009) means. This suggests that CALIOP extinction may be used as a better parameter for estimating $PM_{2.5}$ concentrations from a 2-year mean perspective. Also, the algorithm proposed in this study is essentially a semi-physical-based method, and thus the retrieval process can be improved, upon a careful study of the physical parameters used in the process.

3. Spatial and temporal sampling biases, as well as a retrieval bias, are found. Also, several sensitivity studies were conducted, including surface layer height, cloud flag, $PM_{2.5}/PM_{10}$ ratio, relative humidity, and aerosol type. The sensitivity studies highlight the need for accurate aerosol typing for estimating $PM_{2.5}$ concentrations using CALIOP observations.
4. Using surface-based $PM_{2.5}$ at EPA stations alone, the e-folding correlation length for $PM_{2.5}$ concentrations was found to be about 600 km for the CONUS. A regional analysis yielded values of ~300 km and ~700 km for the Western and Eastern CONUS, respectively. Thus, while limited in spatial sampling, measurements from CALIOP may still be used for estimating $PM_{2.5}$ concentrations over the CONUS.

As noted earlier, CALIOP observations are still rather sparse, and concerns related to reported CALIOP aerosol extinction values also exist, such as solar and surface contamination and the "retrieval fill value" issue (e.g., Toth et al., 2018). Yet, the future High Spectral Resolution Lidar (HSRL) instrument on board the Earth Clouds, Aerosol, and Radiation Explorer (EarthCARE) satellite (Illingworth et al., 2015), as well as forthcoming space-based lidar missions in response to the 2017 Decadal Survey, offer opportunities to further explore aerosol extinction - based PM concentrations. Ultimately the results from this study show that the combined use of several lidar instruments for monitoring regional and global PM pollution is potentially achievable.

Acknowledgements

This research was funded with the support of the NASA Earth and Space Science Fellowship program (NNX16A066H). Author JZ acknowledges the support from NASA grant NNX17AG52G. CALIPSO data were obtained from the NASA Langley Research Center Atmospheric Science Data Center (eos-web.larc.nasa.gov). MODIS data were obtained from NASA Goddard Space Flight Center (ladsweb.nascom.nasa.gov). The $PM_{2.5}$ data were obtained from the EPA AQS site (https://aqs.epa.gov/aqsweb/airdata/download_files.html).

References

Anderson, T.L., Charlson, R. J., Winker, D.M., Ogren, J.A., and Holmén, K.: Mesoscale Variations of Tropospheric Aerosols, J. Atmos. Sci., 60, 119–136, https://doi.org/10.1175/1520-0469(2003)060<0119:MVOTA>2.0.CO;2, 2003.

Atwood, S. A., J. S. Reid, S. M. Kreidenweis, S. S. Cliff, Y. Zhao, N.-H. Lin, S.-C.Tsay, Y.-C. Chu, and Westphal, D.L.: Size resolved measurements of springtime aerosol particles over the northern South China Sea, Atmospheric Environment, 78, 134-143, https://doi.org/10.1016/j.atmosenv.2012.11.024, 2013.

Campbell, J. R., Tackett, J. L., Reid, J. S., Zhang, J., Curtis, C. A., Hyer, E. J., Sessions, W. R., Westphal, D. L., Prospero, J. M., Welton, E. J., Omar, A. H., Vaughan, M. A., and Winker, D. M.: Evaluating nighttime CALIOP 0.532 μm aerosol optical depth and extinction coefficient retrievals, Atmos. Meas. Tech., 5, 2143-2160, https://doi.org/10.5194/amt-5-2143-2012, 2012.

Charlson, R. J., Ahlquist, N. C., and Horvath, H.: On the generality of correlation of atmospheric aerosol mass concentration and light scatter, Atmospheric Environment, 2(5), 455-464, https://doi.org/10.1016/0004-6981(68)90039-5, 1968.

Chew, B. N., Campbell, J. R., Hyer, E. J., Salinas, S. V., Reid, J. S., Welton, E. J., Holben, B.N. and Liew, S. C.: Relationship between aerosol optical depth and particulate matter over Singapore: Effects of aerosol vertical distributions, Aerosol and Air Quality Research, 16, 2818-2830, https://doi.org/10.4209/aaqr.2015.07.0457, 2016.

Chow, J. C., Watson, J. G., Park, K., Robinson, N. F., Lowenthal, D. H., Park, K., and Magliano, K. A.: Comparison of particle light scattering and fine particulate matter mass in central California, Journal of the Air & Waste Management Association, 56(4), 398-410, https://doi.org/10.1080/10473289.2006.10464515, 2006.

Chung, A., Chang, D. P., Kleeman, M. J., Perry, K. D., Cahill, T. A., Dutcher, D., ... & Stroud, K: Comparison of real-time instruments used to monitor airborne particulate matter, Journal of the Air & Waste Management Association, 51(1), 109-120, 2001.

Colarco, P. R., Kahn, R. A., Remer, L. A., and Levy, R. C.: Impact of satellite viewing-swath width on global and regional aerosol optical thickness statistics and trends, Atmos. Meas. Tech., 7, 2313-2335, https://doi.org/10.5194/amt-7-2313-2014, 2014.

Deming, W.E.: Statistical Adjustment of Data, Wiley: New York, 1943.

Di, Q., Wang, Y., Zanobetti, A., Wang, Y., Koutrakis, P., Choirat, C., ... and Schwartz, J. D.: Air pollution and mortality in the Medicare population, New England Journal of Medicine, 376(26), 2513-2522, doi: 10.1056/NEJMoa170274, 2017.

Eatough, D. J., Long, R. W., Modey, W. K., and Eatough, N. L.: Semi-volatile secondary organic aerosol in urban atmospheres: meeting a measurement challenge, Atmospheric Environment, 37(9-10), 1277-1292, 2003.

Engel-Cox, J. A., Holloman, C. H., Coutant, B. W., and Hoff, R. M.: Qualitative and quantitative evaluation of MODIS satellite sensor data for regional and urban scale air quality, Atmos. Environ., 38, 2495–2509, https://doi.org/10.1016/j.atmosenv.2004.01.039, 2004.

Federal Register: National ambient air quality standards for particulate matter. Final Rule Federal Register/vol. 62, no. 138/18 July 1997/Final Rule, 40 CFR Part 50, 1997.

Glantz, P., Kokhanovsky, A., von Hoyningen-Huene, W., and Johansson, C.: Estimating PM2.5 over southern Sweden using space-borne optical measurements, Atmospheric Environment, 43(36), 5838-5846, https://doi.org/10.1016/j.atmosenv.2009.05.017, 2009.

Gong, W., Huang, Y., Zhang, T., Zhu, Z., Ji, Y., and Xiang, H.: Impact and Suggestion of

577 Column-to-Surface Vertical Correction Scheme on the Relationship between Satellite
578 AOD and Ground-Level PM2.5 in China, Remote Sensing, 9(10), 1038,
579 https://doi.org/10.3390/rs9101038, 2017.
580 Greenstone, M.: The impacts of environmental regulations on industrial activity: Evidence from
581 the 1970 and 1977 clean air act amendments and the census of manufactures, Journal of
582 political economy, 110(6), 1175-1219, https://doi.org/10.1086/342808, 2002.
583 Hand, J. L., and Malm, W. C.: Review of aerosol mass scattering efficiencies from ground-
584 based measurements since 1990, Journal of Geophysical Research:
585 Atmospheres, 112(D16), https://doi.org/10.1029/2007JD008484, 2007.
586 Hand, J. L., Schichtel, B. A., Malm, W. C., and Frank, N. H.: Spatial and temporal trends in PM2.5
587 organic and elemental carbon across the United States, Advances in
588 Meteorology, http://dx.doi.org/10.1155/2013/367674, 2013.
589 Hänel, G.: The properties of atmospheric aerosol particles as functions of the relative humidity at
590 thermodynamic equilibrium with the surrounding moist air, Advances in geophysics, 19,
591 73-188, https://doi.org/10.1016/S0065-2687(08)60142-9, 1976.
592 Hess, M., Koepke, P., and Schult, I.: Optical properties of aerosols and clouds: The software
593 package OPAC, Bulletin of the American meteorological society, 79(5), 831-844,
594 https://doi.org/10.1175/1520-0477(1998)079%3C0831:OPOAAC%3E2.0.CO;2, 1998.
595 Hoff, Raymond M., and Christopher, Sundar A.: Remote sensing of particulate pollution from
596 space: have we reached the promised land?, Journal of the Air & Waste Management
597 Association, 59.6 (2009): 645-675, https://doi.org/10.3155/1047-3289.59.6.645, 2009.
598 Huang, X. H., Bian, Q., Ng, W. M., Louie, P. K., and Yu, J. Z: Characterization of PM2.5 major

components and source investigation in suburban Hong Kong: a one year monitoring study, Aerosol Air Qual. Res, 14(1), 237-250, 2014.

Hunt, W. H., Winker, D. M., Vaughan, M. A., Powell, K. A., Lucker, P. L., and Weimer, C.: CALIPSO lidar description and performance assessment, Journal of Atmospheric and Oceanic Technology, 26(7), 1214-1228, https://doi.org/10.1175/2009JTECHA1223.1, 2009.

Illingworth, Anthony J., et al.: The EarthCARE satellite: The next step forward in global measurements of clouds, aerosols, precipitation, and radiation, Bulletin of the American Meteorological Society, 96.8, 1311-1332, https://doi.org/10.1175/BAMS-D-12-00227.1, 2015.

Kaku, K. C., Reid, J. S., Hand, J. L., Edgerton, E. S., Holben, B. N., Zhang, J., and Holz, R. E.: Assessing the challenges of surface-level aerosol mass estimates from remote sensing during the SEAC4RS and SEARCH campaigns: Baseline surface observations and remote sensing in the southeastern United States, Journal of Geophysical Research: Atmospheres, 123, 7530–7562, https://doi.org/10.1029/2017JD028074, 2018.

Kiss, G., Imre, K., Molnár, Á., and Gelencsér, A.: Bias caused by water adsorption in hourly PM measurements, Atmos. Meas. Tech., 10, 2477-2484, https://doi.org/10.5194/amt-10-2477-2017, 2017.

Kittaka, C., Winker, D. M., Vaughan, M. A., Omar, A., & Remer, L. A.: Intercomparison of column aerosol optical depths from CALIPSO and MODIS-Aqua, Atmospheric Measurement Techniques, 4(2), 131, https://doi.org/10.5194/amt-4-131-2011, 2011.

Kumar, N., Chu, A., and Foster, A.: An empirical relationship between PM2.5 and aerosol optical

621 depth in Delhi Metropolitan, Atmos. Environ., 41, 4492–4503,
622 https://doi.org/10.1016/j.atmosenv.2007.01.046, 2007.
623 Levy, R. C., Mattoo, S., Munchak, L. A., Remer, L. A., Sayer, A. M., Patadia, F., and Hsu, N.C.:
624 The Collection 6 MODIS aerosol products over land and ocean, Atmos. Meas. Tech., 6,
625 2989-3034, https://doi.org/10.5194/amt-6-2989-2013, 2013.
626 Li, J., Carlson, B. E., and Lacis, A. A.: How well do satellite AOD observations represent the
627 spatial and temporal variability of PM2.5 concentration for the United States?,
628 Atmospheric environment, 102, 260-273, https://doi.org/10.1016/j.atmosenv.2014.12.010,
629 2015.
630 Liu, Y., Franklin, M., Kahn, R., and Koutrakis, P.: Using aerosol optical thickness to predict
631 ground-level PM2.5 concentrations in the St. Louis area: A comparison between MISR and
632 MODIS, Remote sensing of Environment, 107(1-2), 33-44,
633 https://doi.org/10.1016/j.rse.2006.05.022, 2007.
634 Liu, Y., Park, R. J., Jacob, D. J., Li, Q., Kilaru, V., and Sarnat, J. A.: Mapping annual mean ground-
635 level PM2. 5 concentrations using Multiangle Imaging Spectroradiometer aerosol optical
636 thickness over the contiguous United States, Journal of Geophysical Research:
637 Atmospheres, 109 (D22), https://doi.org/10.1029/2004JD005025, 2004.
638 Liu, Y., Sarnat, J. A., Kilaru, V., Jacob, D. J., and Koutrakis, P.: Estimating ground-level PM2.5
639 in the eastern United States using satellite remote sensing, Environmental science &
640 technology, 39(9), 3269-3278, doi: 10.1021/es049352m, 2005.
641 Liou, Kuo-Nan.: An introduction to atmospheric radiation, Vol. 84. Academic press, 2002.
642 Lynch P., and coauthors: An 11-year global gridded aerosol optical thickness reanalysis (v1.0) for

643 atmospheric and climate sciences, Geosci. Model Dev., 9, 1489-1522, doi:10.5194/gmd-9-
644 1489-2016, 2016.
645 Malm, W.C. and Hand, J.L.: An examination of the physical and optical properties of aerosols
646 collected in the IMPROVE program, Atmospheric Environment, 41(16), pp.3407-3427,
647 https://doi.org/10.1016/j.atmosenv.2006.12.012, 2007.
648 Nessler, R., Weingartner, E., and Baltensperger, U. (2005). Effect of humidity on aerosol light
649 absorption and its implications for extinction and the single scattering albedo illustrated for
650 a site in the lower free troposphere, *Journal of Aerosol Science*, *36*(8), 958-972.
651 Omar, A. H., Winker, D. M., Tackett, J. L., Giles, D. M., Kar, J., Liu, Z., Vaughan, M. A., Powell,
652 K. A., and Trepte, C. R.: CALIOP and AERONET aerosol optical depth comparisons: One
653 size fits none, J. Geophys. Res. Atmos., 118, 4748–4766, doi:10.1002/jgrd.50330, 2013.
654 Patashnick, H., Rupprecht, G., Ambs, J. L., and Meyer, M. B.: Development of a reference
655 standard for particulate matter mass in ambient air, Aerosol Science & Technology, 34(1),
656 42-45, 2001.
657 Reid, J. S., Eck, T. F., Christopher, S. A., Koppmann, R., Dubovik, O., Eleuterio, D. P., Holben,
658 B. N., Reid, E. A., and Zhang, J.: A review of biomass burning emissions part III: intensive
659 optical properties of biomass burning particles, Atmos. Chem. Phys., 5, 827-849,
660 https://doi.org/10.5194/acp-5-827-2005, 2005.
661 Reid, J. S. et al.: Skill of Operational Aerosol Forecast Models in Predicting Aerosol Events and
662 Trends of the Eastern United States, A11B-001, AGU Fall meeting, San Francisco, 12-16
663 Dec, 2016.
664 Reid, J. S., Kuehn, R. E., Holz, R. E., Eloranta, E. W., Kaku, K. C., Kuang, S., ... and Atwood,

S.A.: Ground-based High Spectral Resolution Lidar observation of aerosol vertical distribution in the summertime Southeast United States, Journal of Geophysical Research: Atmospheres, 122(5), 2970-3004, https://doi.org/10.1002/2016JD025798, 2017.

Sessions, W. R., Reid, J. S., Benedetti, A., Colarco, P. R., da Silva, A., Lu, S., Sekiyama, T., Tanaka, T. Y., Baldasano, J. M., Basart, S., Brooks, M. E., Eck, T. F., Iredell, M., Hansen, J. A., Jorba, O. C., Juang, H.-M. H., Lynch, P., Morcrette, J.-J., Moorthi, S., Mulcahy, J., Pradhan, Y., Razinger, M., Sampson, C. B., Wang, J., and Westphal, D. L.: Development towards a global operational aerosol consensus: basic climatological characteristics of the International Cooperative for Aerosol Prediction Multi-Model Ensemble (ICAP-MME), Atmos. Chem. Phys., 15, 335-362, https://doi.org/10.5194/acp-15-335-2015, 2015.

Silva, R. A., West, J. J., Zhang, Y., Anenberg, S. C., Lamarque, J. F., Shindell, D. T., Collins, W.J., Dalsoren, S., Faluvegi, G., Folberth, G. & Horowitz, L. W.: Global premature mortality due to anthropogenic outdoor air pollution and the contribution of past climate change, Environmental Research Letters, 8(3), 034005, doi:10.1088/1748-9326/8/3/034005, 2013.

Spagnolo, G. S.: Automatic instrument for aerosol samples using the beta-particle attenuation, Journal of aerosol science, 20(1), 19-27, 1989.

Toth, T. D., Campbell, J. R., Reid, J. S., Tackett, J. L., Vaughan, M. A., Zhang, J., and Marquis, J. W.: Minimum aerosol layer detection sensitivities and their subsequent impacts on aerosol optical thickness retrievals in CALIPSO level 2 data products, Atmos. Meas. Tech., 11, 499-514, https://doi.org/10.5194/amt-11-499-2018, 2018.

Toth, T. D., Zhang, J., Campbell, J. R., Hyer, E. J., Reid, J. S., Shi, Y., and Westphal, D. L.: Impact

of data quality and surface-to-column representativeness on the $PM_{2.5}$ / satellite AOD relationship for the contiguous United States, Atmos. Chem. Phys., 14, 6049-6062, https://doi.org/10.5194/acp-14-6049-2014, 2014.

Toth, T. D., Zhang, J., Campbell, J. R., Reid, J. S., Shi, Y., Johnson, R. S., Smirnov, A., Vaughan, M.A. and Winker, D. M.: Investigating enhanced Aqua MODIS aerosol optical depth retrievals over the mid-to-high latitude Southern Oceans through intercomparison with co-located CALIOP, MAN, and AERONET data sets, Journal of Geophysical Research: Atmospheres, 118(10), 4700-4714, https://doi.org/10.1002/jgrd.50311, 2013.

Toth, T. D., Zhang, J., Campbell, J. R., Reid, J. S., and Vaughan, M. A.: Temporal variability of aerosol optical thickness vertical distribution observed from CALIOP, Journal of Geophysical Research: Atmospheres, 121(15), 9117-9139, https://doi.org/10.1002/2015JD024668, 2016.

Val Martin, M., Heald, C. L., Ford, B., Prenni, A. J., and Wiedinmyer, C.: A decadal satellite analysis of the origins and impacts of smoke in Colorado, Atmos. Chem. Phys., 13, 7429-7439, https://doi.org/10.5194/acp-13-7429-2013, 2013.

Van Donkelaar, A., Martin, R.V., Brauer, M., Kahn, R., Levy, R., Verduzco, C., and Villeneuve, P. J.: Global Estimates of Ambient Fine Particulate Matter Concentrations from Satellite Based Aerosol Optical Depth: Development and Application, Environ. Health Perspect., 118(6): 847–855, https://dx.doi.org/10.1289%2Fehp.0901623, 2010.

Van Donkelaar, A., Martin, R. V., Spurr, R. J., and Burnett, R. T.: High-resolution satellite-derived PM2.5 from optimal estimation and geographically weighted regression over North America, Environmental science & technology, 49.17 (2015): 10482-10491, doi: 10.1021/acs.est.5b02076, 2015.

710 Waggoner, A. P., and Weiss, R. E.: Comparison of fine particle mass concentration and light
711 scattering extinction in ambient aerosol, Atmospheric Environment (1967), 14(5), 623-
712 626, https://doi.org/10.1016/0004-6981(80)90098-0, 1980.
713 Wang, J., and Christopher, S. A.: Intercomparison between satellite-derived aerosol optical
714 thickness and PM2.5 mass: implications for air quality studies, Geophysical research
715 letters, 30(21), https://doi.org/10.1029/2003GL018174, 2003.
716 Winker, D. M., Hunt, W. H., and McGill, M. J.: Initial performance assessment of CALIOP,
717 Geophysical Research Letters, 34(19), https://doi.org/10.1029/2007GL030135, 2007.
718 Winker, D. M., Pelon, J., Coakley Jr, J. A., Ackerman, S. A., Charlson, R. J., Colarco, P. R., ...
719 and Kubar, T. L.: The CALIPSO mission: A global 3D view of aerosols and clouds,
720 Bulletin of the American Meteorological Society, 91(9), 1211-1230,
721 https://doi.org/10.1175/2010BAMS3009.1, 2010.
722 Winker, D. M., Vaughan, M. A., Omar, A., Hu, Y., Powell, K. A., Liu, Z., Hunt, W. H., and Young,
723 S. A.: Overview of the CALIPSO Mission and CALIOP Data Processing Algorithms, J.
724 Atmos. Oceanic Technol., 26, 2310–2323, https://doi.org/10.1175/2009JTECHA1281.1,
725 2009.
726 Young, S. A., Vaughan, M. A., Kuehn, R. E., and Winker, D. M.: The retrieval of profiles of
727 particulate extinction from Cloud–Aerosol Lidar and Infrared Pathfinder Satellite
728 Observations (CALIPSO) data: Uncertainty and error sensitivity analyses, Journal of
729 Atmospheric and Oceanic Technology, 30(3), 395-428,
730 https://doi.org/10.1175/2009JTECHA1281.1, 2013.
731 Zhang, J., Campbell, J.R., Hyer, E. J., Reid, J.S., Westphal, D. L., and Johnson, R. S.: Evaluating

the impact of multisensor data assimilation on a global aerosol particle transport model, J. Geophys. Res. Atmos., 119, 4674–4689, doi:10.1002/2013JD020975, 2014.

Zhang, J. and Reid, J.S.: An analysis of clear sky and contextual biases using an operational over ocean MODIS aerosol product, Geophysical Research Letters, 36, L15824, doi:10.1029/2009GL038723, 2009.

Figure and Table Captions

Figure 1. For 2008-2009, scatterplot of mean $PM_{2.5}$ concentration from ground-based U.S. EPA stations and mean column AOD (550 nm) from collocated Collection 6 (C6) Aqua MODIS observations. The red line represents the Deming regression fit.

Figure 2. For 2008-2009 over the CONUS, (a) mean $PM_{2.5}$ concentration ($\mu g\ m^{-3}$) for those U.S. EPA stations with reported daily measurements, and (c) 1° x 1° average CALIOP-derived $PM_{2.5}$ concentrations for the 100–1000 m AGL atmospheric layer, using Equation 3, for combined daytime and nighttime conditions. Also shown are the pairwise $PM_{2.5}$ concentrations from (b) EPA daily measurements and (d) those derived from CALIOP (day and night combined), both averaged for each EPA station for the 2008-2009 period. For all four plots, values greater than 20 μgm^{-3} are colored red.

Figure 3. For 2008-2009 over the CONUS, 1° x 1° average CALIOP extinction, relative to the number of cloud-free 5 km CALIOP profiles in each 1° x 1° bin, for the 100 – 1000 m AGL atmospheric layer, for (a) daytime and (b) nighttime measurements. Also shown are the corresponding CALIOP-derived $PM_{2.5}$ concentrations, using Equation 3 for (c) daytime and (d) nighttime conditions. Values greater than 0.2 km^{-1} and 20 $\mu g\ m^{-3}$ for (a, b) and (c, d), respectively, are colored red. Scatterplots of mean $PM_{2.5}$ concentration from ground-based U.S. EPA stations and those derived from collocated near-surface CALIOP observations are shown in the bottom row, using (e) daytime and (f) nighttime CALIOP data. The red lines represent the Deming regression fits.

794 Figure 4. Scatterplot of mean $PM_{2.5}$ concentration from ground-based U.S. EPA stations and those
795 derived from collocated near-surface CALIOP observations using combined daytime and
796 nighttime CALIOP data. The red line represents the Deming regression fit.
797
798 Figure 5. Root-mean-square errors of CALIOP-derived $PM_{2.5}$ against EPA $PM_{2.5}$ as a function of
799 CALIOP-derived $PM_{2.5}$, using both daytime (in red) and nighttime (in blue) CALIOP observations.
800 The five bins are equally sampled based upon a cumulative histogram analysis, and each point
801 from left to right represents the RMSE and mean $PM_{2.5}$ concentration derived from CALIOP for
802 0-20%, 20-40%, 40-60%, 60-80%, and 80-100% cumulative frequencies.
803
804 Figure 6. Two-year (2008-2009) histograms of mean $PM_{2.5}$ concentrations from the U.S. EPA (in
805 black) and those derived from aerosol extinction using nighttime (in blue) and daytime (in red)
806 CALIOP data. The U.S. EPA data shown are not collocated, while those derived using CALIOP
807 are spatially (but not temporally) collocated, with EPA station observations.
808
809 Figure 7. Two-year (2008-2009) histograms of mean $PM_{2.5}$ concentrations from the U.S. EPA and
810 those derived from spatially and temporally collocated aerosol extinction using (a) daytime and
811 (b) nighttime CALIOP data.
812
813 Figure 8. For 2008-2009, scatterplots of mean $PM_{2.5}$ concentration from ground-based U.S. EPA
814 stations and mean column AOD from collocated CALIOP observations, using (a) daytime and (b)
815 nighttime CALIOP data. The red lines represent the Deming regression fits.
816

817 Figure 9. For 2008-2009, scatterplots of mean $PM_{2.5}$ concentration from ground-based U.S. EPA
818 stations and those derived from collocated all-sky (including cloud-free and cloudy profiles) near-
819 surface CALIOP observations, using (a) daytime and (b) nighttime CALIOP data. The red lines
820 represent the Deming regression fits.
821
822 Figure 10. For 2008-2009 over the CONUS, scatterplot of distance (km) between any two U.S.
823 EPA stations and the corresponding spatial correlation of $PM_{2.5}$ concentration between each pair
824 of stations. The black curve represents the exponential fit to the data for the entire CONUS, and
825 the red and blue dashed lines represent 10 km bin averages for the Western and Eastern CONUS,
826 respectively.
827
828 Table 1. The parameters, and corresponding values, used to quality assure the CALIOP aerosol
829 extinction profile.
830
831 Table 2. Statistical summary of a sensitivity analysis varying the height of the surface layer,
832 including R^2, slope from Deming regression, mean bias (CALIOP - EPA) of $PM_{2.5}$ in $\mu g\ m^{-3}$, and
833 percent error change in derived $PM_{2.5,}$ defined as: ((mean new $PM_{2.5}$ – mean original $PM_{2.5}$)/mean
834 original $PM_{2.5}$)*100. The row in bold represents the results shown in the remainder of the paper.
835
836 Table 3. Statistical summary of a sensitivity analysis varying the $PM_{2.5}$ to PM_{10} ratio used,
837 including slope from Deming regression, mean bias (CALIOP - EPA) of $PM_{2.5}$ in $\mu g\ m^{-3}$, and
838 percent error change in derived $PM_{2.5,}$ defined as: ((mean new $PM_{2.5}$ – mean original $PM_{2.5}$)/mean
839 original $PM_{2.5}$)*100. The row in bold represents the results shown in the remainder of the paper.

Table 4. Statistical summary of a sensitivity analysis varying the aerosol type assumed in the derivation of $PM_{2.5}$, including R^2, slope from Deming regression, mean bias (CALIOP - EPA) of $PM_{2.5}$ in $\mu g\ m^{-3}$, and percent error change in derived $PM_{2.5}$, defined as: ((mean new $PM_{2.5}$ – mean original $PM_{2.5}$)/mean original $PM_{2.5}$)*100. The row in bold represents the results shown in the remainder of the paper.

Appendix Figure 1. For 2008-2009 over the CONUS, for each 1° x 1° grid box, the number of days and CALIOP Level 2 5 km aerosol profiles used in the creation of the maps in Fig. 3 for (a, c) daytime and (b, d) nighttime measurements. Values greater than 400 profiles for (c, d) are colored red.

869 **Figures**

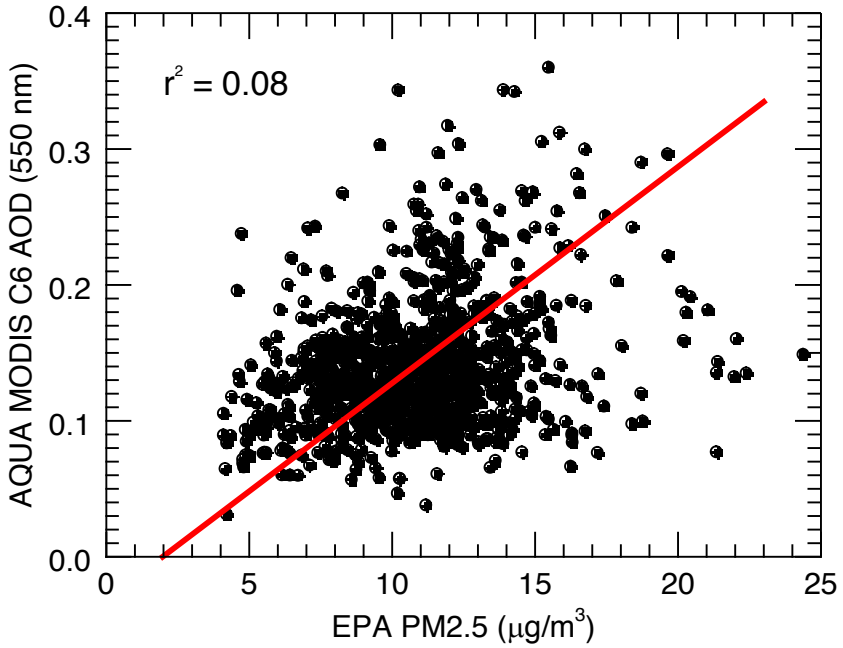

Figure 1. For 2008-2009, scatterplot of mean $PM_{2.5}$ concentration from ground-based U.S. EPA stations and mean column AOD (550 nm) from collocated Collection 6 (C6) Aqua MODIS observations. The red line represents the Deming regression fit.

870

871

872

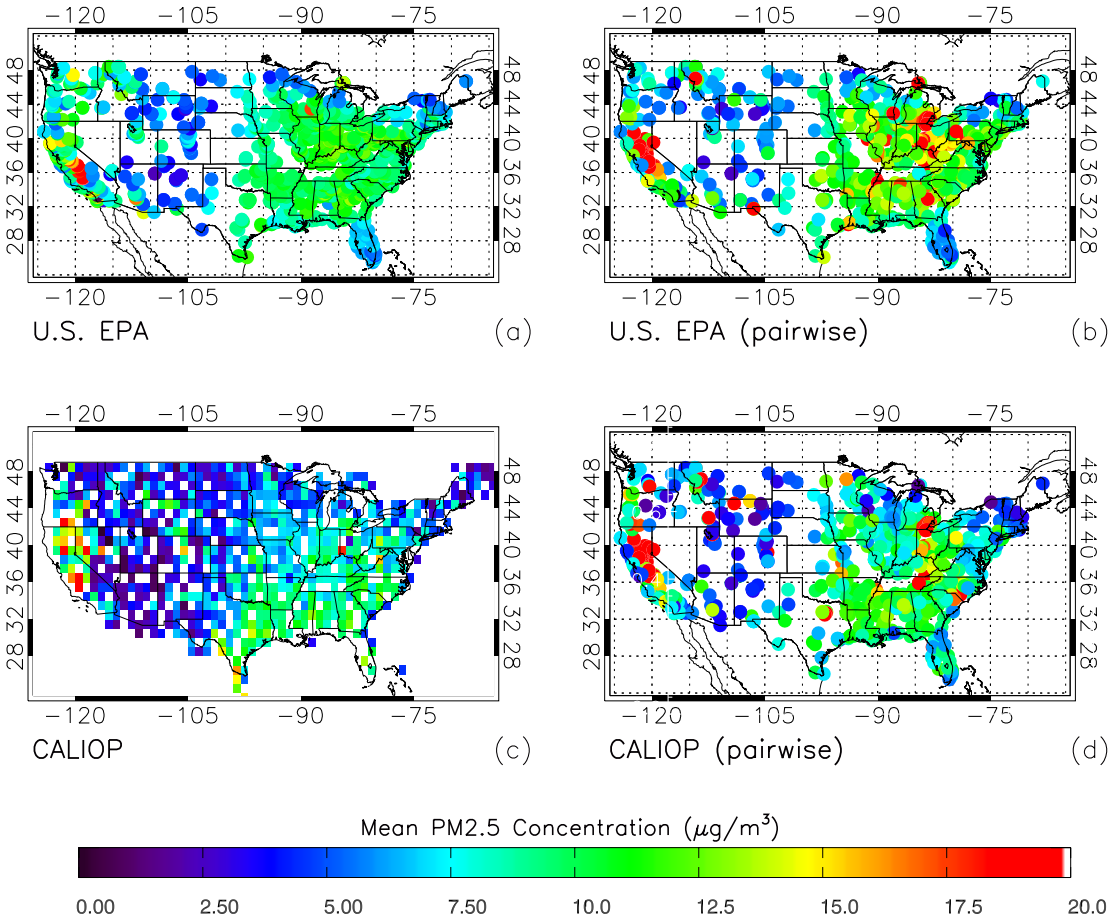

Figure 2. For 2008-2009 over the CONUS, (a) mean $PM_{2.5}$ concentration (μg m^{-3}) for those U.S. EPA stations with reported daily measurements, and (c) 1° x 1° average CALIOP-derived $PM_{2.5}$ concentrations for the 100–1000 m AGL atmospheric layer, using Equation 3, for combined daytime and nighttime conditions. Also shown are the pairwise $PM_{2.5}$ concentrations from (b) EPA daily measurements and (d) those derived from CALIOP (day and night combined), both averaged for each EPA station for the 2008-2009 period. For all four plots, values greater than 20 μg m^{-3} are colored red.

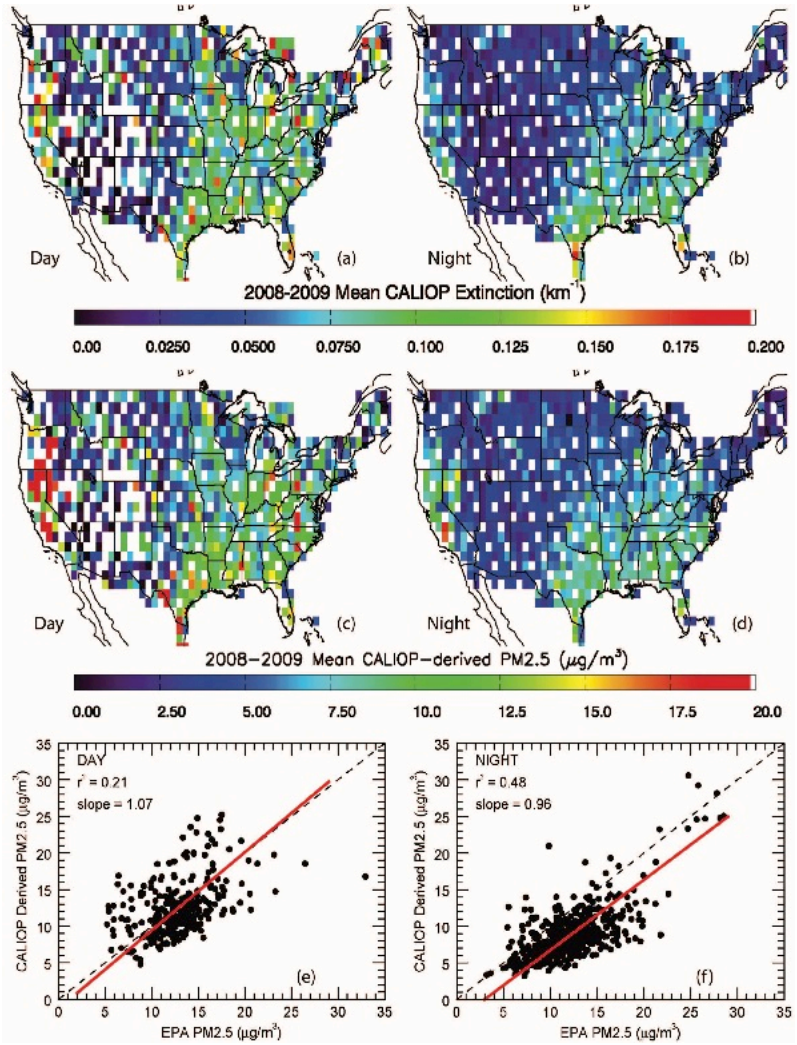

Figure 3. For 2008-2009 over the CONUS, 1° x 1° average CALIOP extinction, relative to the number of cloud-free L2_05kmAPro profiles in each 1° x 1° bin, for the 100 – 1000 m AGL atmospheric layer, for (a) daytime and (b) nighttime measurements. Also shown are the corresponding CALIOP-derived $PM_{2.5}$ concentrations, using Equation 3 for (c) daytime and (d) nighttime conditions. Values greater than 0.2 km^{-1} and 20 $\mu g\ m^{-3}$ for (a, b) and (c, d), respectively, are colored red. Scatterplots of mean $PM_{2.5}$ concentration from ground-based U.S. EPA stations and those derived from collocated near-surface CALIOP observations are shown in the bottom row, using (e) daytime and (f) nighttime CALIOP data. The red lines represent the Deming regression fits.

873

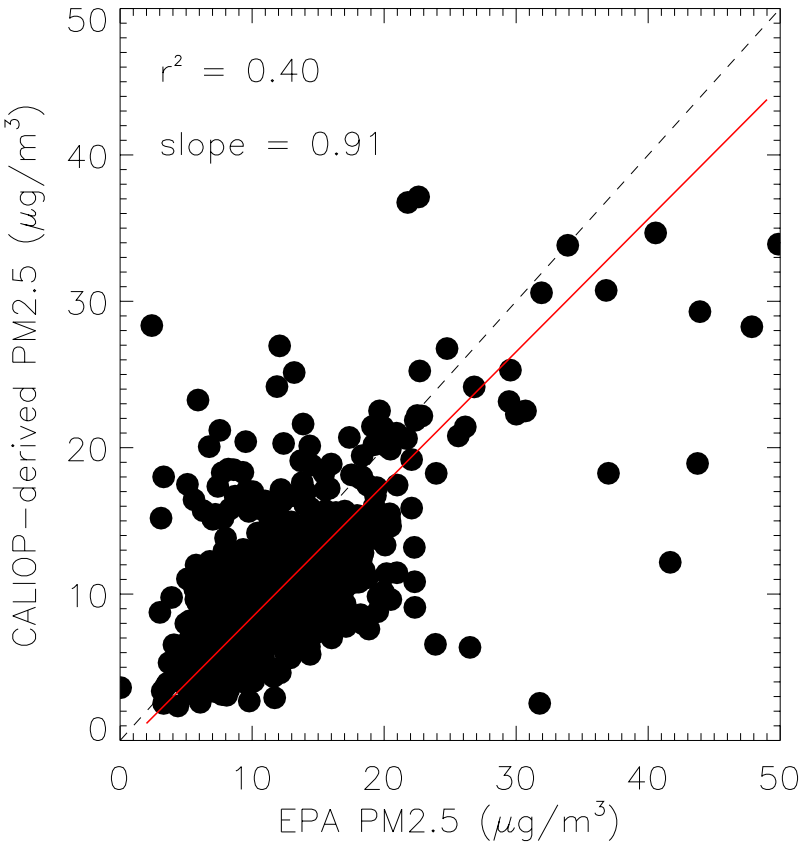

Figure 4. Scatterplot of mean $PM_{2.5}$ concentration from ground-based U.S. EPA stations and those derived from collocated near-surface CALIOP observations using combined daytime and nighttime CALIOP data. The red line represents the Deming regression fit.

874

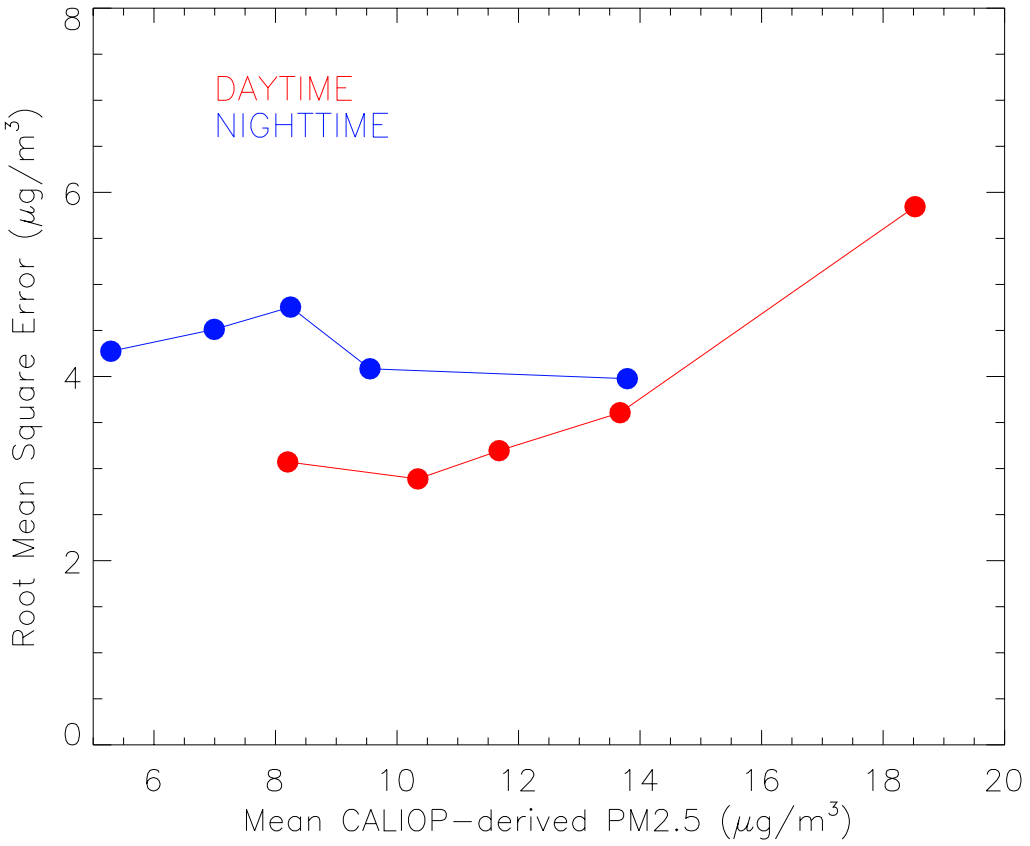

Figure 5. Root-mean-square errors of CALIOP-derived $PM_{2.5}$ against EPA $PM_{2.5}$ as a function of CALIOP-derived $PM_{2.5}$, using both daytime (in red) and nighttime (in blue) CALIOP observations. The five bins are equally sampled based upon a cumulative histogram analysis, and each point from left to right represents the RMSE and mean $PM_{2.5}$ concentration derived from CALIOP for 0-20%, 20-40%, 40-60%, 60-80%, and 80-100% cumulative frequencies.

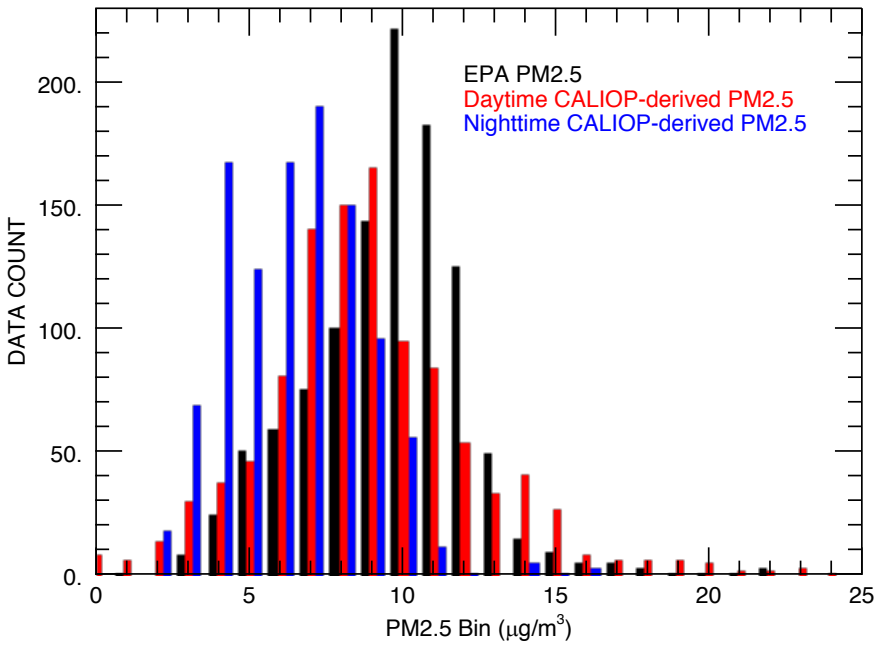

Figure 6. Two-year (2008-2009) histograms of mean $PM_{2.5}$ concentrations from the U.S. EPA (in black) and those derived from aerosol extinction using nighttime (in blue) and daytime (in red) CALIOP data. The U.S. EPA data shown are not collocated, while those derived using CALIOP are spatially (but not temporally) collocated, with EPA station observations.

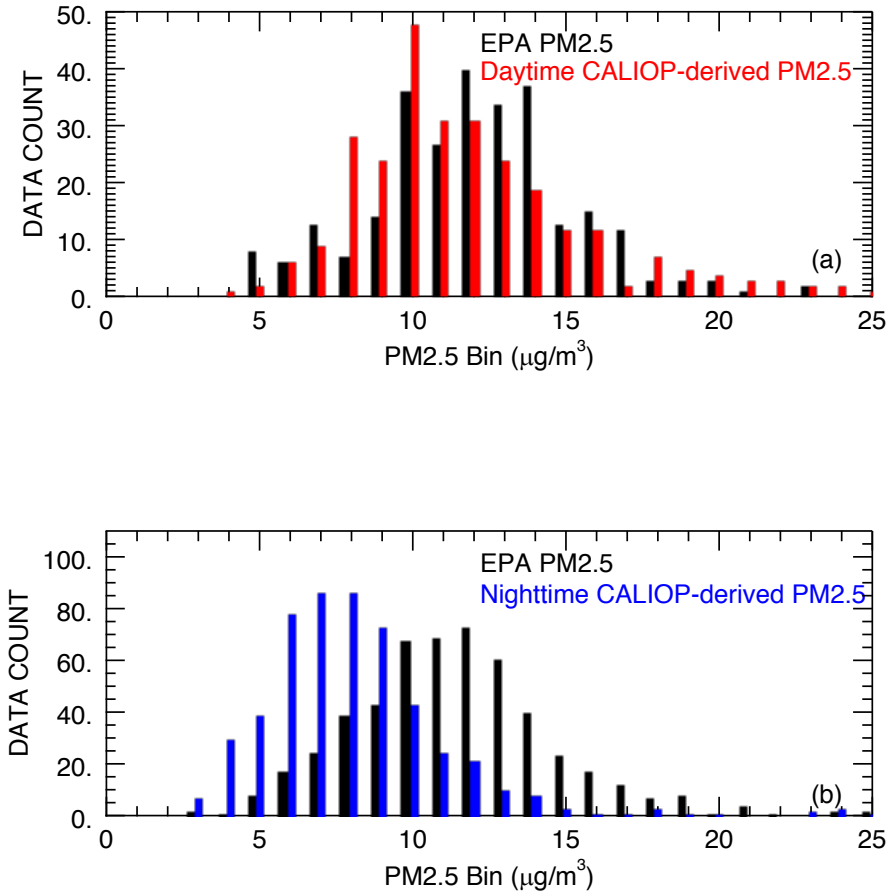

Figure 7. Two-year (2008-2009) histograms of mean $PM_{2.5}$ concentrations from the U.S. EPA and those derived from spatially and temporally collocated aerosol extinction using (a) daytime and (b) nighttime CALIOP data.

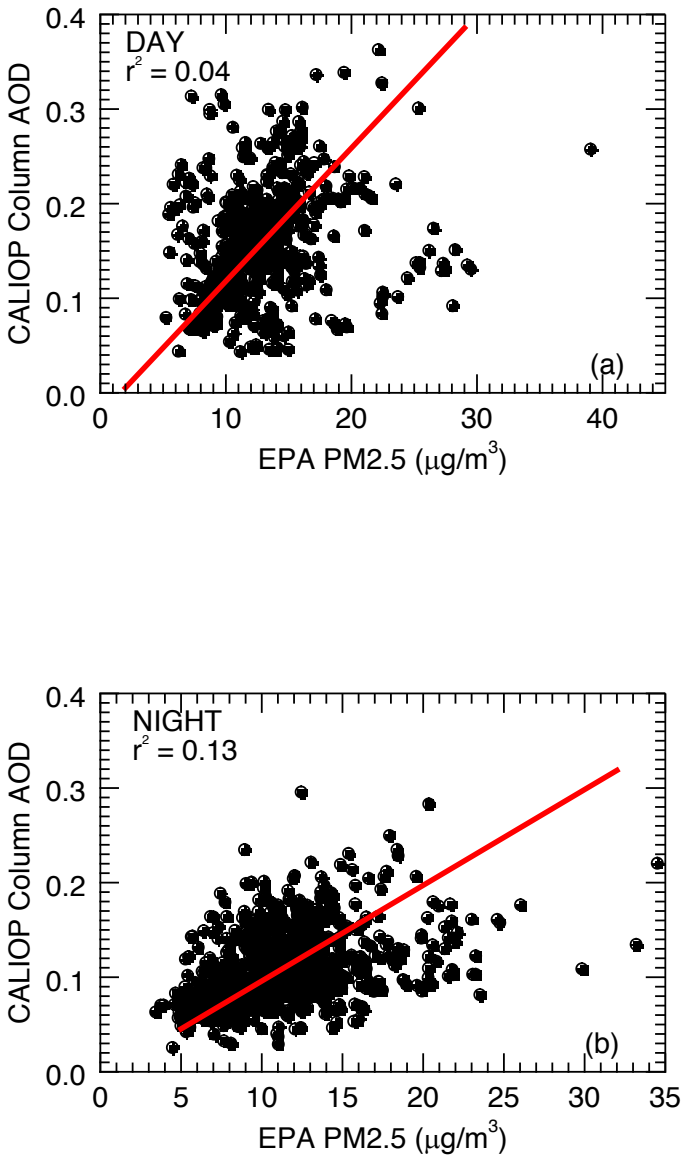

Figure 8. For 2008-2009, scatterplots of mean $PM_{2.5}$ concentration from ground-based U.S. EPA stations and mean column AOD from collocated CALIOP observations, using (a) daytime and (b) nighttime CALIOP data. The red lines represent the Deming regression fits.

902
903

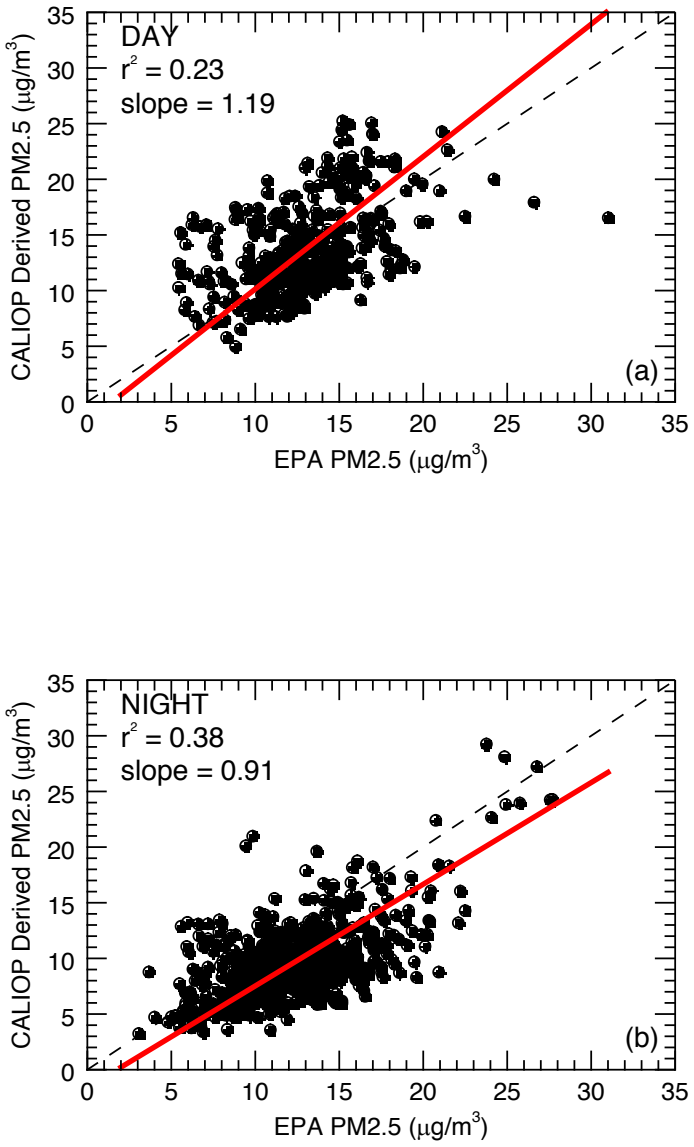

Figure 9. For 2008-2009, scatterplots of mean $PM_{2.5}$ concentration from ground-based U.S. EPA stations and those derived from collocated all-sky (including cloud-free and cloudy profiles) near-surface CALIOP observations, using (a) daytime and (b) nighttime CALIOP data. The red lines represent the Deming regression fits.

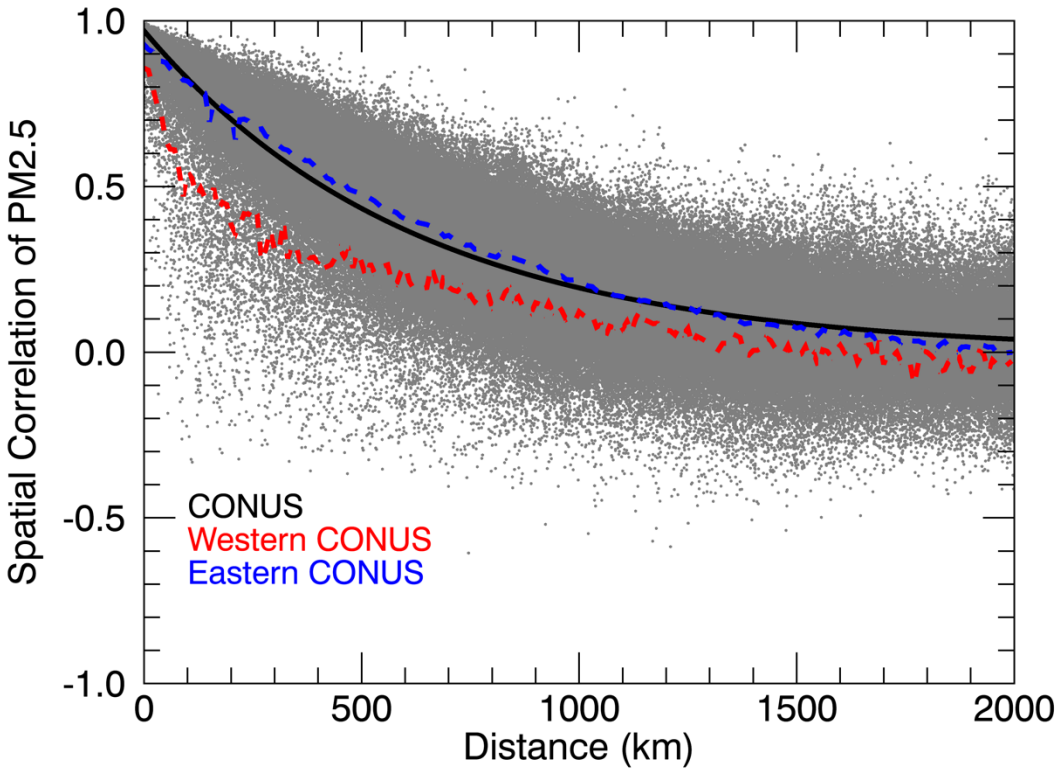

Figure 10. For 2008-2009 over the CONUS, scatterplot of distance (km) between any two U.S. EPA stations and the corresponding spatial correlation of $PM_{2.5}$ concentration between each pair of stations. The black curve represents the exponential fit to the data for the entire CONUS, and the red and blue dashed lines represent 10 km bin averages for the Western and Eastern CONUS, respectively.

908
909
910
911

912
913 **Tables**
914
915
916

Parameter	Values
Integrated_Attenuated_Backscatter_532	≤ 0.01 sr^{-1}
Extinction_Coefficient_532	≥ 0 and ≤ 1.25 km^{-1}
Extinction_QC_532	= 0, 1, 2, 16, or 18
CAD_Score	≥ -100 and ≤ -20
Extinction_Coefficient_Uncertainty_532	≤ 10 km^{-1}
Atmospheric_Volume_Description (Bits 1-3)	= 3
Atmospheric_Volume_Description (Bits 10-12)	$\neq 0$

Table 1. The parameters, and corresponding values, used to quality assure the CALIOP aerosol extinction profile.

917
918
919
920
921
922
923
924
925
926

Surface Layer (m)	Analysis (Day/Night)			
	R^2	**Deming Slope**	**Mean Bias (CALIOP - EPA; μg m^{-3})**	**Error Change (%)**
0-100	0.27/0.41	1.32/0.60	-2.67/-9.06	-13.71/-61.94
0-200	0.33/0.53	1.34/1.04	-0.52/-5.68	3.79/-23.58
0-300	0.35/0.54	1.32/1.11	-0.09/-4.70	7.24/-12.15
0-400	0.38/0.57	1.30/1.13	-0.13/-4.25	6.92/-6.46
0-500	0.35/0.52	1.26/1.06	-0.21/-4.04	5.70/-4.39
0-600	0.40/0.53	1.19/1.04	-0.46/-3.91	3.72/-2.15
0-700	0.44/0.46	1.20/0.98	-0.41/-3.89	2.73/-2.88
0-800	0.35/0.50	1.06/0.94	-0.59/-3.76	-0.77/-2.04
0-900	0.17/0.49	1.04/0.91	-0.74/-3.74	-3.91/-2.25
0-1000	0.13/0.48	0.98/0.89	-1.08/-3.74	-7.48/-2.57
100-500	0.34/0.44	1.23/1.00	0.54/-3.40	14.21/-0.84
100-1000	**0.21/0.48**	**1.07/0.96**	**-0.39/-3.34**	

Table 2. Statistical summary of a sensitivity analysis varying the height of the surface layer, including R^2, slope from Deming regression, mean bias (CALIOP - EPA) of $PM_{2.5}$ in μg m^{-3}, and percent error change in derived $PM_{2.5}$, defined as: ((mean new $PM_{2.5}$ – mean original $PM_{2.5}$)/mean original $PM_{2.5}$)*100. The row in bold represents the results shown in the remainder of the paper.

	Analysis (Day/Night)		
$PM_{2.5}/PM_{10}$ Ratio	**Deming Slope**	**Mean Bias (CALIOP - EPA; µg m^{-3})**	**% Error Change**
Low ratio (-1 STDEV) = 0.24	0.43/0.38	-7.81/-8.61	-60.00%/-60.00%
High ratio (+1 STDEV) = 0.88	1.57/1.41	5.39/0.77	46.67%/46.67%
0.6	**1.07/0.96**	**-0.39/-3.34**	

Table 3. Statistical summary of a sensitivity analysis varying the $PM_{2.5}$ to PM_{10} ratio used, including slope from Deming regression, mean bias (CALIOP - EPA) of $PM_{2.5}$ in µg m^{-3}, and percent error change in derived $PM_{2.5}$, defined as: ((mean new $PM_{2.5}$ – mean original $PM_{2.5}$)/mean original $PM_{2.5}$)*100. The row in bold represents the results shown in the remainder of the paper.

Analysis (Day/Night)							
Aerosol Type				**R^2**	**Deming Slope**	**Mean Bias (CALIOP - EPA; µg m^{-3})**	**% Error Change**
	a_{scat}	a_{abs}	Γ				
Smoke	5.26	0.26	0.18	0.10/0.44	0.86/0.78	-1.81/-4.26	-11.53/-10.54
Sea salt	1.42	0.01	0.46	0.18/0.48	2.92/2.64	22.42/12.93	184.12/184.99
Dust	0.52	0.08	0.00	0.05/0.39	9.01/8.18	102.04/70.82	826.94/843.33
Sulfate	**3.4**	**0.37**	**0.63**	**0.21/0.48**	**1.07/0.96**	**-0.39/-3.34**	

Table 4. Statistical summary of a sensitivity analysis varying the aerosol type assumed in the derivation of $PM_{2.5}$, including R^2, slope from Deming regression, mean bias (CALIOP - EPA) of $PM_{2.5}$ in µg m^{-3}, and percent error change in derived $PM_{2.5}$, defined as: ((mean new $PM_{2.5}$ – mean original $PM_{2.5}$)/mean original $PM_{2.5}$)*100. The row in bold represents the results shown in the remainder of the paper.

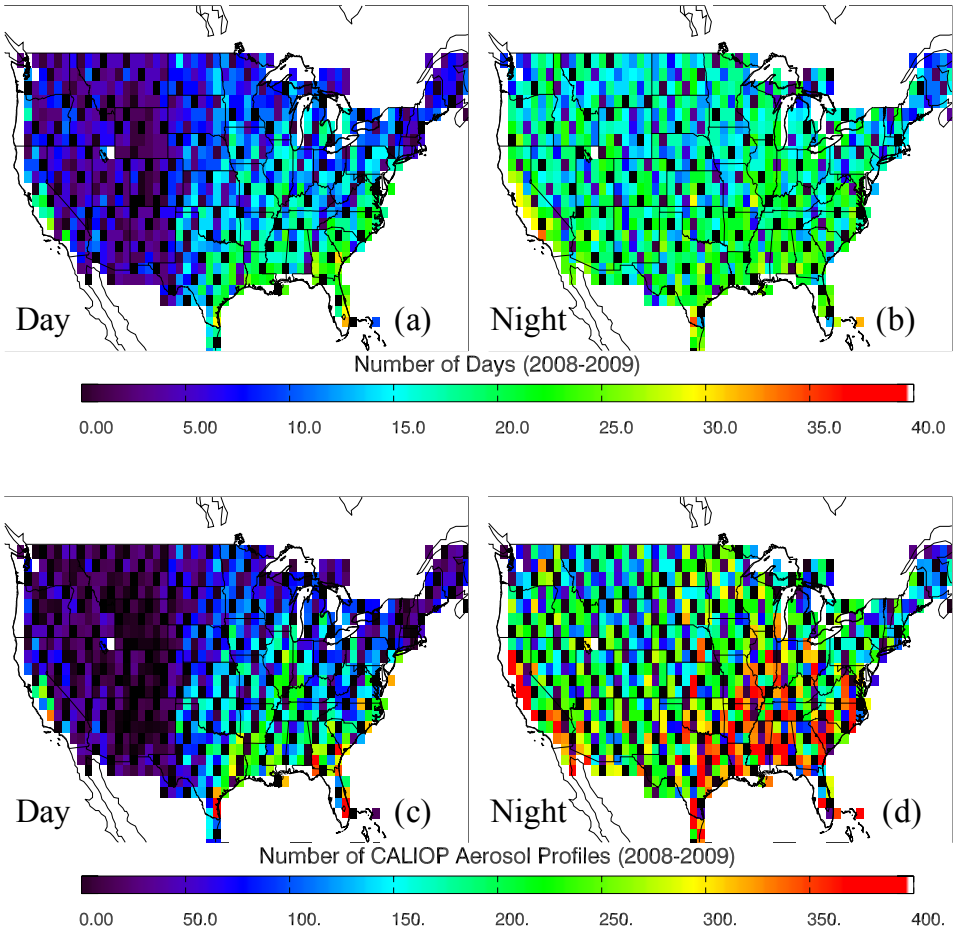

Appendix Figure 1. For 2008-2009 over the CONUS, for each 1° x 1° grid box, the number of days and CALIOP Level 2 5 km aerosol profiles used in the creation of the maps in Fig. 3 for (a, c) daytime and (b, d) nighttime measurements. Values greater than 400 profiles for (c, d) are colored red.

959
960
961